Bioorganic & Medicinal Chemistry xxx (xxxx) xxxx

Contents lists available at ScienceDirect

Bioorganic & Medicinal Chemistry

journal homepage: www.elsevier.com/locate/bmc

Anti-inflammatory effect and inhibition of nitric oxide production by targeting COXs and iNOS enzymes with the 1,2-diphenylbenzimidazole pharmacophore

Mónica I. García-Aranda[a], Jazmin E. Gonzalez-Padilla[c], Carlos Z. Gómez-Castro[d], Yolanda M. Gómez-Gómez[a], Martha C. Rosales-Hernández[c], Efrén V. García-Báez[a], Marina O. Franco-Hernández[a], José L. Castrejón-Flores[b,*], Itzia I. Padilla-Martínez[a,*]

[a] Laboratorio de Química Supramolecular y Nanociencias, Unidad Profesional Interdisciplinaria de Biotecnología del Instituto Politécnico Nacional, Av. Acueducto s/n Barrio la Laguna Ticomán, Ciudad de México 07340, Mexico City, Mexico
[b] Laboratorio de Cultivo Celular y Biología Molecular, Unidad Profesional Interdisciplinaria de Biotecnología del Instituto Politécnico Nacional, Av. Acueducto s/n Barrio la Laguna Ticomán, Ciudad de México 07340, Mexico City, Mexico
[c] Laboratorio de Biofísica y Biocatálisis, Sección de Estudios de Posgrado e Investigación, Escuela Superior de Medicina del Instituto Politécnico Nacional, Plan de San Luis y Díaz Mirón s/n, Casco de Santo Tomás, 11340 Mexico City, Mexico
[d] CONACyT – Universidad Autónoma del Estado de Hidalgo, km 4.5 Carretera Pachuca-Tulancingo, Col. Carboneras, Mineral de la Reforma, Hidalgo 42184, Mexico

ARTICLE INFO

Keywords:
Benzimidazole
Anti-inflammatory
COX-inhibition
iNOS inhibition
Interaction profile of COX-2

ABSTRACT

Being the base of several non-communicable diseases, including cancer, inflammation is a complex process generated by tissue damage or change in the body homeostatic state. Currently, the therapeutic treatment for chronic inflammation related diseases is based on the use of selective cyclooxygenase II enzyme, COX-2, inhibitors or Coxibs, which have recently regained attention giving their preventive role in colon cancer. Thus, the discovery of new molecules that selectively inhibit COX-2 and other inflammatory mediators is a current challenge in the medicinal chemistry field. 1-Phenylbenzimidazoles have shown potential COX inhibitory activity, because they can reproduce the interaction profile of known COX inhibitors. Therefore, in the present investigation a series of 1,2-diphenylbenzimidazoles (DPBI) with different aromatic substitutions in the *para* position were synthesized and their interaction with COX-2 and nitric oxide synthase, iNOS, was determined *in silico, in vitro and in vivo*. Compound 2-(4-bromophenyl)-1-(4-nitrophenyl)-1*H*-benzo[*d*]imidazole showed the best inhibition towards COX-2, while compounds *N*-(4-(2-(4-bromophenyl)-1*H*-benzo[*d*]imidazol-1-yl)phenyl) acetamide and *N*-(4-(2-(4-chlorophenyl)-1*H*-benzo[*d*]imidazol-1-yl)phenyl)acetamide diminished the production of NO *in vitro*. Additionally, they had a significant anti-inflammatory activity *in vivo* when given orally.

1. Introduction.

Inflammation is the base of several non-communicable diseases, which kills 41 million people each year representing the 71% of all the global deaths according with the World Health Organization.[1] Several drugs targeting different receptors are currently used as anti-inflammatory agents, and can be classified as steroidal, non-steroidal drugs (NSAIDs) or agent modifiers of the diseases, which includes biological drugs such as antibodies. Among them, NSAIDs are widely and commonly used. They inhibit, non-selectively, the action of the cyclooxygenases (COX-1 and COX-2) enzymes decreasing the production of prostaglandins (PGs), although their chronic use correlates with the presence of gastric ulcers as a result of the dysregulation in gastric acid inhibition and mucosal production regulated by PGs.

At the beginning of the new century, the development of selective COX-2 inhibitors opened a new horizon for the treatment of chronic inflammation associated diseases making a breakthrough in the control of inflammation.[2] COX-2 is highly expressed during the inflammatory response, although recent reports have shown that it is also constitutively expressed in other organs.[3] Unfortunately, COX-2 inhibitors were not free of adverse effects and their prolonged use, more than five years, resulted in myocardial infarction in a few patients leading to the withdrawn of certain coxibs and the restriction in their use. However, recent clinical studies have confronted previous findings demonstrating their safety.[4] A renewed interest in the use of coxibs has arisen, because it has been shown that their use together with other anti-carcinogenic

* Corresponding authors.
E-mail addresses: jlcastrejon@ipn.mx (J.L. Castrejón-Flores), ipadillamar@ipn.mx (I.I. Padilla-Martínez).

https://doi.org/10.1016/j.bmc.2020.115427
Received 17 December 2019; Received in revised form 2 March 2020; Accepted 5 March 2020

drugs might help to prevent colon cancer.[5] Nonetheless, the COX-2 inhibition effect and its relationship with cancer prevention needs to be further investigated into detail.

A vast amount of research has been focused exclusively in the inhibition of COX-1 or −2 as modifiers agents of the inflammatory process, and although it has been proved very effective, this process is a complex phenomenon with several cells and effector molecules involved. For example, nitric oxide (NO) is a small but potent pro-inflammatory molecule secreted during inflammation that causes vasodilation and cellular migration, and at higher concentrations, it downregulates adhesion molecules and induce apoptosis of inflammatory cells. Inducible nitric oxide synthase or iNOS, a target for drug designing, is expressed by macrophages and transforms L-arginine into NO and L-citrulline.[6,7]

The benzimidazole ring (BI), a benzene and imidazole fused structure, is a widely used pharmacophore with a myriad of clinical applications including diseases with an inflammatory etiology.[8] Substituted-BI structures are not structurally related to NSAIDs or selective COX-2 inhibitors, although they have shown a similar inhibition profile than these commercial drugs given their capacity to bind to similar sites and mimic interaction patterns than NSAIDs.[9] Pioneering work with 2-substituted-BI, -benzothiazole and -benzoxazole heterocycles showed that the BI ring had a moderate selective inhibition against human COX-2 when compared with the other heterocycles.[10] Moreover, a series of 5-substitued-1-phenylsulfonyl-2-methylbenzimidazole compounds showed moderate anti-inflammatory effect when tested in a rat edema *in vivo* assay, but their effect over COX-2 inhibition was not established.[11] More recently, 2-coumarin-BI series were evaluated as anti-inflammatory compounds *in vivo* demonstrating a good inhibitory effect in the rat paw edema model, where the withdrawing groups in the aromatic ring seem to benefit the anti-inflammatory effect.[12] Additionally, the benzimidazole heterocycle, particularly 5-chloro-1,3-dihydro-2*H*-benzimidazol-2-one, showed a potent NO inhibition, which varies upon the different substitutions, although the effect of a double phenyl substitution to the core benzimidazole ring and their effect towards iNOS has not been assessed.

Therefore, following previous findings published by our group demonstrating the affinity of 1-phenylbenzimidazole derivatives towards COXs enzymes,[9] the synthesis of a novel family of 1,2-diphenylbenzimidazole (DPBI) substituted compounds was achieved with the aim to profiling them as selective COXs and iNOS inhibitors by *in vitro* and *in vivo* assays. The results demonstrate that the DPBI substitution with strong and weak electro withdrawing groups not only resulted in a significant inhibition towards COX-2, but also in an important anti-inflammatory effect *in vivo*, while the acetamide substitution diminished the production of NO. Moreover, 2-(4-bromophenyl)-1-(4-nitrophenyl)-1*H*-benzo[*d*]imidazole reduced inflammation when administrated orally in rats.

2. Results and discussion.

2.1. Route of synthesis of the DPBI substituted compounds.

The synthetic pathways employed for the synthesis of the intermediate and final compounds are depicted in Scheme 1. In the initial step, the synthesis of compounds **1a-e** was carried out by the condensation reaction between 1,2-phenylenediamine and the corresponding aromatic aldehyde with excellent yields (90–97%). In a second step, the N1 position of the compounds was substituted accomplishing an aromatic nucleophilic substitution reaction, using 1-fluoro-4-nitrobenzene as nucleophile in basic media, to obtain compounds **2a-e**[13] with moderate to good yields (52–82%). The set of compounds **3** was obtained through the reduction of the NO_2 group to NH_2, with Sn in acidic medium,[14] which were further acetylated to generate the series of compounds **4**, in both cases with high yields (90–95%).

The ^{1}H NMR data of the series of compounds **2**, **3** and **4** showed four signals, for each of the protons of the benzofused ring, and four more for the eight protons of the *p*-substituted *C*2-Ph and N1-Ph rings. Their chemical shifts were the expected in agreement with the electro-donor (ED) or electro-withdrawing (EW) nature of the substituents. For the acetylated compounds **4**, the characteristic signal for the NH and Me groups were also observed at low and high frequencies, respectively. Finally, ^{13}C NMR data confirmed the structures. The chemical shifts of *C*2 are almost independent of the nature of the substituents appearing in the 149.8–152.4 range, whereas the δ of the ipso C13 and C19 depend on the EW or ED nature of the substituents, as the most relevant features. Furthermore, the stretching bands (cm^{-1}) of the nitrile, acid and amide groups were clearly observed in the IR spectra of compounds **2a** (νCN = 2225 cm^{-1}), **2f** (νCO = 1707 cm^{-1}) and **4** (νCO = 1707–1667 cm^{-1}, νNH = 3465–3251 cm^{-1}).

Compound **2c** crystallized in the triclinic form, space group *P*-1 (No.2) with two molecules in the unit cell. The molecular structure of compound **2c**, shown in Figure 1(a), is similar to the bromine derivative **2b**, reported elsewhere.[13] The *C*2-Ph and N1-Ph rings are out of the mean plane formed by the BI-heterocycle by 19.95(4)° and 58.08(3)°, respectively, and the torsion angle between the two planes is 68.14(4)°. The strong EW effect of the *p*-NO_2 group, in the N1-Ph ring, is responsible of most of the non covalent dispersive interactions observed in the crystal network, such as C—H···A (A = π, N, O) and ONO··· π in addition to the Cl··· π interaction that rise the supramolecular structure (Figure 1(b) and Table S1 (Supporting Information)). The *ab initio* MKS[15] calculated charges for the N1-Ph hydrogens were in 1.50 to 1.80 range, in agreement with their involvement in C—H···A dispersive interactions (Table S2). Theoretical calculations underscore the importance of enhanced electrostatic stabilization in the non-covalent interactions in the crystal structure.

2.2. Docking computational analysis.

2.2.1. Predicted COX-1 and −2 affinity of the DPBI-substituted compounds.

From the molecular docking calculations an estimated free energy of binding (ΔG°_b) was obtained for the set of DPBIs and the control compounds in both COX-1 and COX-2 models. The number of binding modes (BM) found inside the COX binding site, the lowest free energy of binding (ΔG°_b), and the selectivity indices for COX-2 are listed in Table 1. These results show that the estimated activity of the tested compounds is comparable to the control inhibitors, while in some cases the affinity of the DPBIs is even higher than that calculated for both ibuprofen (Ibp) and etoricoxib (Etox). According to docking calculations, it was observed that all compounds would be more active for COX-2 than for COX-1 with free energies of binding ranging between −8.94 to −10.73 kcal/mol and −6.87 to −9.18 kcal/mol, respectively. From the calculated affinities, the COX-2 selectivity index ($\Delta G^\circ_{b,COX\text{-}2}/\Delta G^\circ_{b,COX\text{-}1}$) is higher in the series of compounds **2**, with the *p*-NO_2 substitution at the N1-Ph ring, than in the analogous compounds of the series **3** and **4**.

2.2.2. COX binding modes of DPBI substituted compounds.

The calculated COX-inhibitor complexes, indicate that all compounds bind to COX-1 through a single binding mode or BM-I, see Figure 2(a). In this conformation, the inhibitors simultaneously occupy three relevant pockets within the COX binding site, i.e. the stereoselective pocket close to the entrance of the COX binding site, the long hydrophobic COX channel, and the side pocket. This last is associated to the binding of Coxibs, while the other two bind all the classic NSAIDs as well. By comparing the binding pose of the studied inhibitors with the crystallographic structure Ibp, it can be observed that the benzo-fused ring of the BI occupies the same space as the chiral isopropyl moiety of Ibp, interacting closely with residues Leu359, Val316, and Tyr355. The longest axis of the compounds, i.e. the BI-*C*2-Ph moiety, was aligned

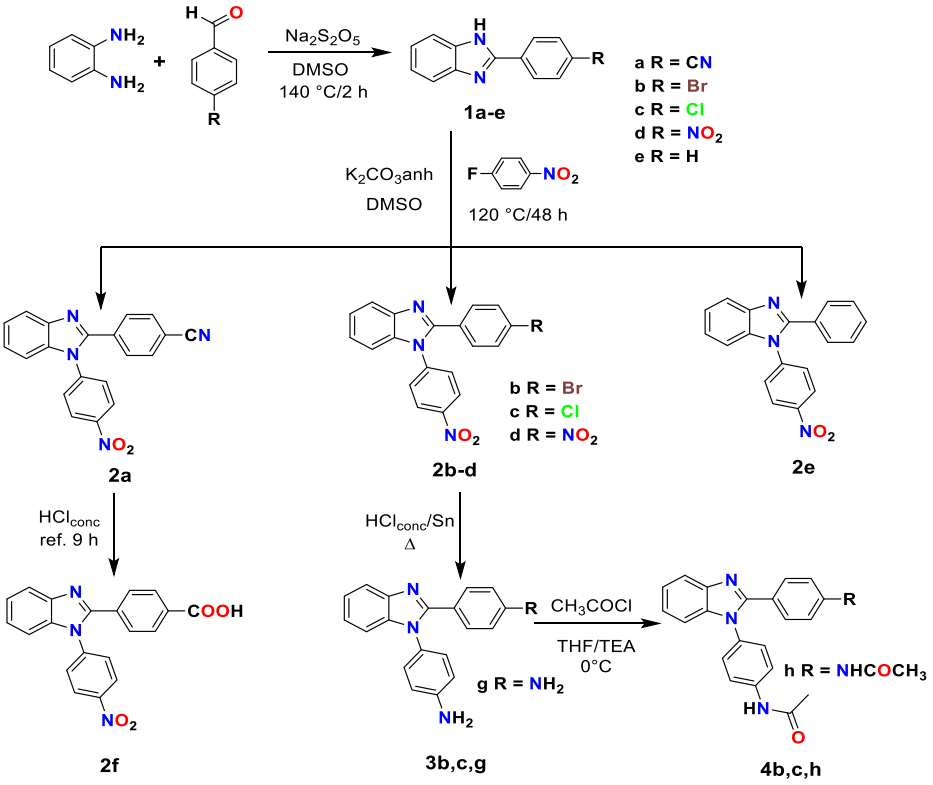

Scheme 1. Chemical route for the synthesis of 1,2-diphenilbenzimidazole (DPBI) substituted compounds defined as **2a-f**, **3b,c,g** and **4b,c,h.**

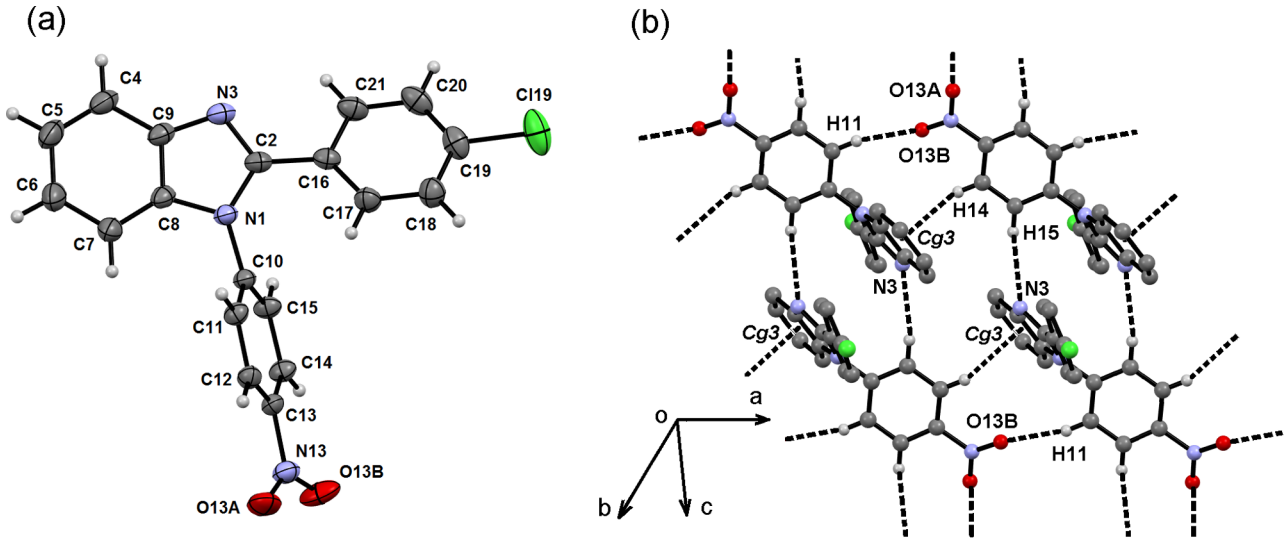

Figure 1. (a) Ortep of compound **2c** at 50% probability level. (b) Two-dimensional supramolecular architecture in the (0 8–5) plane.

along the COX channel placing the functional group in close contact with Met522, Trp387 and Tyr385 residues, at the top of the hydrophobic channel. The N1-Ph moiety of the model compounds was, in most cases, able to bind the side pocket, reaching residues such as His90, Gln192, Phe518, and Ile523; this last residue is known to shrink the access to the side channel in COX-1, whereas, its substitution to Val in COX-2 allows the access to the side pocket for many Coxibs.[16]

It is important to note that the above described BM-I was actually unfavorable for the compound series **2** in COX-1, because several non-COX binding modes were actually more stable than those found within the COX binding site for this series (data not shown). For series **3**, the N1-Ph rings binds to the side pocket of COX-1 but with low affinity. The reduced calculated affinity of all compounds for COX-1 is due to the inaccessibility of the BM-I to the COX-1 side pocket, however the $NHCOCH_3$ substitution at the N1-Ph ring in compound series **4** was able to access to the side pocket in COX-1 with increased affinity, see Table 1.

The BMs found for COX-2 included the BM-I described in COX-1 only in the case of *para*-substituted compounds with Br or Cl at the *C*2-Ph ring, i.e., compound series **b** and **c**, along with compound **2e**, unsubstituted at the same ring, see Figure 2(b). The fact that the rest of the compounds with different functional groups were unable to reproduce the BM-I in COX-2 reflects the selectivity of this isoform for halogen atoms at the top of the hydrophobic channel, a feature that can be exploited to achieve selectivity. Nevertheless, all the tested compounds showed alternative binding modes in COX-2 besides the one shared

Table 1
Docking results for Ibuprofen, Etoricoxib and DPBIs **2a-f**, **3b,c,g** and **4b,c,h** with COX-1 and COX-2.

Compound	Number of COX binding modes (BM)		ΔG°_b (kcal/mol)		Selectivity index	
	COX-1	COX-2	COX-1	COX-2	$\Delta G^{\circ}_{b,COX-2}/\Delta G^{\circ}_{b,COX-1}$	$K_{d,COX-2}/K_{d,COX-1}$
2a	1	2	−7.29	−10.65	1.46	0.0034
2b	1	4	−7.42	−9.87	1.33	0.0160
2c	1	2	−7.26	−9.85	1.36	0.0126
2d	1	2	−6.87	−10.17	1.48	0.0038
2e	0	3	NA	−9.48	NA	NA
2f	0	3	NA	−9.84	NA	NA
3b	2	3	−8.33	−9.24	1.11	0.2153
3c	1	4	−8.01	−9.17	1.14	0.1412
3g	1	1	−7.02	−8.94	1.27	0.0391
4b	1	4	−9.18	−10.73	1.17	0.0731
4c	1	3	−8.97	−10.69	1.19	0.0549
4h	1	2	−9.09	−10.26	1.13	0.1388
Ibuprofen	1	1	−8.31	−7.16	0.86	6.9658
Etoricoxib	2	3	−7.57	−10.47	1.38	0.0075

NA = Not Available

with COX-1 as predicted from previous computational calculations by the research group.[9] Relative to N1-phenylbenzimidazoles, the addition of the second substituting phenyl ring at the BI center increases selectivity and reduces the number of binding modes. The alternative binding modes in COX-2 occupy the three COX pockets already mentioned but flipping each of the three vertices of the molecules. Five out of six possible binding modes (I-V) were observed in the calculations, see Figure 2(b-f). Considering the energetics together with a knowledge-based criteria, a selection of the most plausible BM for each complex was performed as specified in Table S3 and described in the next section.

2.2.3. Interaction profile of DPBI relative to known inhibitor complexes.

To rule out alternative BMs the Ligand-Receptor Contact Distance (LRCD) parameter was used as a measure of similarity in the interaction profile of enzyme-inhibitor complexes.[9] The strategy consisted in selecting the BM that maximized the similarity in the pattern of interactions relative to know inhibitors co-crystallized with the COX enzymes. Briefly, we performed a search in the PDB finding 74 crystallographic COX-inhibitor complexes (24 for COX-1 and 50 for COX-2) for which the LRCD was calculated against each of the calculated complexes in the docking calculations. The LRCD scores were ranked for each DPBI, COX isoform and BM; Table S4 lists the combination of crystallographic complex and BM that produced the lowest LRCD score for each compound. Thus, the best match for each compound determined the BM considered to be the most representative among the distribution observed in COX-2 (highlighted in Table S3) as an alternative criterion to the ΔG°_b.

It is worth noting that the best matches found in the data base of reference complexes included Celecoxib complexes with either COX-1 or COX-2 as well as complexes of Indomethacin derivatives known to occupy the side pocket of COX-1.[18] The followed knowledge-based criteria suggest that compound series **2**, would bind COX-2 preferentially through BM-III or BM-IV, whereas series **3** and **4** would bind through BM-II and BM-V, respectively. These matches generally point to the lowest energy BMs, except for compound series **4**, for this series the energy criteria select BM-I whereas the knowledge-based criteria points to BM-V. This discrepancy may be solved by considering the *in vitro* assessment on COX enzymes presented later; compound series **4** showed selective COX-1 inhibition which may be explained by a change in the binding mode in both isoforms. As already mentioned, the calculations showed that this series are active for COX-1 due to the capability of the N1-Ph ring and its acetamide group to interact with the side pocket of this isoform. Therefore, a change in the binding mode from BM-I to BM-V would explain the observed activity since BM-V in COX-2 does not keep the key interactions observed in COX-1. Thus, these results suggest that the specificity of the binding mode in each of the compound series is a key factor to explain the inhibitory profile and selectivity of the studied DPBI compounds.

2.3. Pharmacological evaluation of the DPBI substituted compounds.

2.3.1. Evaluation of the cytotoxic activity in vitro.

Before any functional assay, the effect of all compounds over the viability of the macrophage cell line RAW 264.7 was determined by the change in the metabolic activity, as a readout of viability, using the MTT assay. The compounds of the series **3**, (*p*-NH_2 group in the N1-Ph) were the less cytotoxic, maintaining 80% viability or more, at the highest concentration tested (500 μM), above this concentration most compounds were not soluble. In contrast, the series of compounds **2** (*p*-NO_2 group in the N1-Ph) were more cytotoxic. In fact, compound **2d**, with a double *p*-NO_2 substitution, exhibited the highest cytotoxicity, reducing viability to less than half at 500 μM. The high toxicity seen with the NO_2 substituted benzimidazoles has been positively related with *in vitro* toxicity in tumoral cells lines as a result of the inhibition of

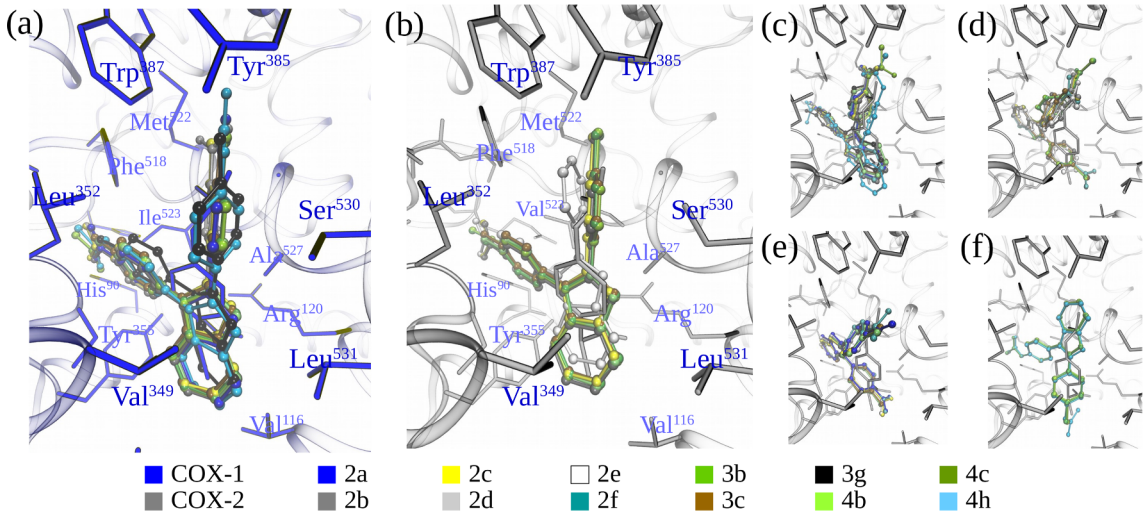

Figure 2. Binding modes found for DPBI-substituted in COX-1 and COX-2. (a) Complexes of compounds in binding mode I with COX-1. (b)-(f) Complexes of compounds in binding modes I-V in COX-2, respectively. See Table S3 for a list of the specific molecules in each binding mode.

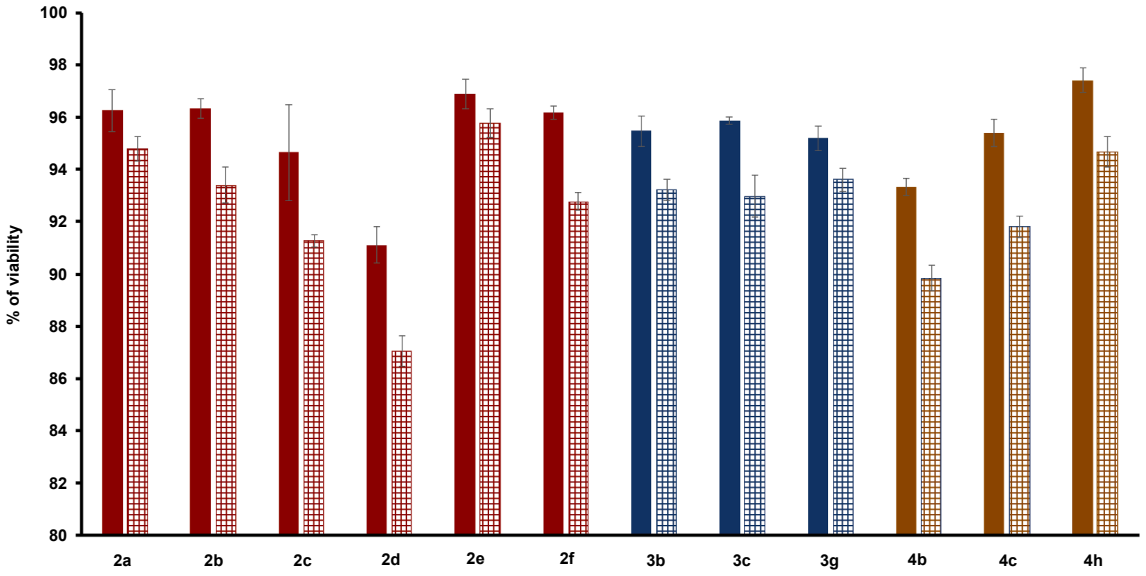

Figure 3. Cytotoxic activity *in vitro* of the DPBI-substituted compounds over murine macrophages at pharmacological relevant concentrations. Results are present as the mean ± standard deviation of a triplicate of three independent experiments at concentration of 50 (solid bars) and 100 (grid bars) μM.

the PARPs enzymes.[17] Moreover, NO_2 substituted compounds can transform to the nitroso reactive compound, formed during NO_2 reduction, a powerful electrophile that reacts with proteins and DNA.[18,19]

After evaluating the cytotoxicity, the *in vitro* therapeutic concentration, defined as the concentration at which the viability remains at 90%, was established, see Figure 3. Almost all compounds, but **2d**, kept viability up to 90% at 100 μM, so further experiments were executed using this maximal concentration or below.

2.3.2. *In vitro inhibition of COX-1 and COX-2 enzymes.*

The COXs inhibition assay was performed with all the compounds including commercial drugs at a concentration of 100 μM for direct comparison. Ibp, Etox and the kit selective inhibitor compounds, SC-560 and DUP-697, were used as selective inhibitors for COX-1 and −2. As expected, the SC-560 and DUP-697, compounds showed a potent inhibition, 94% and 84%, for COX-1 and −2, respectively, validating the assay. Ibp and Etox did cause selective inhibition of 54% and 63% over COX-1 and −2, respectively, and the selectivity index (SI), the ratio between COX-2 and COX-1 activities, was obtained for Etox (SI = 2.68) and Ibp (SI = 0.96). Although the computational studies showed a preference interaction of all the compound with COX-2, some of the compounds had a strong inhibition towards COX-1, which was higher than Ibp, see Table 2. The *in vitro* assays validate the docking findings demonstrating that compounds of series **2** had the strongest affinity towards COX-2. Among them, compound **2b** and **2d**, showed the highest percentages of inhibition towards COX-2, 51% and 48%, respectively. Compound **2b** had the best *in vitro* inhibition, 51%, which is lower than the inhibition seen with Etox, 62%. Although having the best inhibitory parameters including a high affinity towards COX-2 in silico, the compounds in series 2 exhibited a medium to low potency towards the therapeutic target. Importantly, compound **2b** was less selective towards COX-1 which resulted in a slightly higher selectivity index (SI = 2.77) than Etox (Table 2). The anti-inflammatory activity of a *C*2-Ph substitution in the BI ring, particularly, the 2-(1*H*-benzo[*d*]imidazole-2-yl)-*N*-(2,3-dimethylphenyl)benzamine was previously assessed showing a weak selective inhibition towards COX-2 (SI = 0.651).[20] Thus, the N1-Ph substitution in the BI is a decisive factor not only strengthening COX-2 inhibition, but also reducing the specificity for COX-1, in the tested compounds. According with the binding modes studies, the N1-Ph substitution will bind to the side pocket, a particular structural feature of the COX-2 enzyme,

Table 2
Selective Inhibitory activity and IC_{50} concentration of DPBIs against COX-1 and COX-2 enzymes.

Compounds	% of Enzyme Inhibition		Selectivity	IC_{50} μM	
	COX-2	COX-1	SI	COX-2	COX-1
2a	34.3 ± 1.1	29.0 ± 0.2	1.63	–	–
2b	50.8 ± 1.1	18.3 ± 0.4	2.77	102	–
2c	23.3 ± 0.6	17.6 ± 0.8	1.37	–	–
2d	47.7 ± 1.0	29.3 ± 0.7	1.63	–	–
2e	42.7 ± 0.3	40.6 ± 0.5	1.05	162	175
2f	32.8 ± 0.7	31.0 ± 1.4	1.06	–	–
3b	17.6 ± 0.8	62.3 ± 0.7	0.11	–	–
3c	44.8 ± 3.3	39.0 ± 0.4	1.15	193	224
3g	45.9 ± 0.8	29.7 ± 1.1	1.55	173	–
4b	28.4 ± 1.0	48.7 ± 0.8	0.58	–	–
4c	23.8 ± 1.6	47.4 ± 1.0	0.51	–	–
4h	27.0 ± 4.4	59.5 ± 0.2	0.53	–	–
Etoricoxib	62.6 ± 0.8	23.4 ± 1.3	2.68	–	–
Ibuprofen	53.7 ± 0.5	56.6 ± 1.2	0.96	–	–

Cyclooxygenases 1 and 2 = COX-1, COX-2, SI = Selectivity Index (COX-2/COX-1), IC_{50} = Half maximal inhibitory concentration.

demonstrating the relevance of this substitution over the *C*2-Ph analogues. Additionally, the halogenated *para* substitution at the N1-Ph synergized the inhibition by interacting directly with another relevant COX binding site, such as the long hydrophobic COX channel.

2.3.3. *Inhibition of NO production.*

The capacity of the compounds to inhibit the production of nitric oxide was assessed in murine macrophages activated with LPS at therapeutic concentrations. Thus, the cells were incubated at 50 μM and 100 μM to determine the potency and dose dependent effect of the tested compounds, see Table 3. Interestingly, most compounds showed better inhibition at the lowest concentration, suggesting dose dependent effect of the molecules over the pharmacological target. Compound **2b**, which showed the best inhibition over COX-2, was not the best in reducing NO production, suggesting that this result is not directly related with the decrease of COX-2 activity. On the contrary, compounds **4b** and **4c** reduced the NO production at the levels observed with the commercial drugs. Structurally, compounds **4b** and **4c**, had both an acetamide group in the *para* position and a *para* halogenated at N1-Ph and *C*2-Ph, respectively.

Table 3
In vitro inhibition of NO production of the DPBIs compounds in macrophages stimulated with LPS.

Compounds	% Nitric Oxide inhibition	
	50 μM	100 μM
2a	24.4 ± 8.9	46.0 ± 6.8
2b	46.5 ± 6.7	45.8 ± 5.8
2c	53.2 ± 5.7	53.9 ± 6.4
2d	22.4 ± 9.6	33.8 ± 6.8
2e	38.1 ± 6.2	44.0 ± 4.5
2f	32.6 ± 7.8	46.2 ± 7.6
3b	62.5 ± 7.3	74.2 ± 2.8
3c	24.9 ± 7.5	52.2 ± 5.2
3g	42.5 ± 6.9	44.1 ± 7.3
4b	77.3 ± 5.3	83.6 ± 6.1
4c	75.9 ± 3.7	86.4 ± 1.9
4h	10.1 ± 4.4	15.3 ± 7.0
Etoricoxib	79.8 ± 1.9	87.3 ± 1.4
Ibuprofen	82.1 ± 1.9	83.7 ± 2.8

Results are represented as the mean ± standard deviation of a triplicate of three independent experiments.

Most synthetic NO inhibitors are competitive inhibitors of L-arginine which is the natural substrate of the inducible nitric oxide synthase enzyme (iNOS). The acetamide group, present in compounds of the series **4**, has been highlighted as potent iNOS inhibitor. This group in the C5 position of indole derivatives, resulted highly specific showing only inhibition towards iNOS, but not against the constitutively expressed neural and endothelial forms. These compounds interact directly with the active site of iNOS blocking the enzymatic reaction that leads to NO production.[21] In order to enlighten the mechanism of NO inhibition in the presence of the 1,2-DPBIs *in vitro*, docking calculations of the best inhibitory compounds, **4b** and **4c,** were performed on h-iNOS. The resulting free energy of binding (ΔG°_{b} = -8.9 and −9.0 kcal mol^{-1}) and dissociation constant values (K_d = 0.284 and 0.249 μM), calculated for **4b** and **4c**, respectively, are of the same order of magnitude than potent h-iNOS inhibitors.[22] The interaction profiles of **4b** and **4c**, in h-iNOS active site, are depicted in Figure 4. Both compounds are close to the amino acid residues Asp382, Arg388, Gln263, Pro350, Val352, Trp372, Tye373, Glu377. However, compound **4c** is hydrogen bonded with Asp382 and Arg388, whereas compound **4c** is forming hydrophobic interactions with these two amino acids.

2.3.4. Evaluation of the anti-inflammatory activity in vivo

The anti-inflammatory effect of all the compounds (100 mg/kg) was tested using the *in vivo* carrageenan paw animal model, where maximal edema formation, 75% more than the saline solution group, was seen 3 h after the injection of carrageenan. Ibp (100 mg/kg) and Etox (10 mg/kg) reduced edema formation by 42% and 35%, respectively. Importantly, compound **2b** and **2d**, the best COX-2 inhibitors, exhibited better reduction in the edema formation, 42%, which is comparable with the effect of the commercial drugs, see Figure 5. The rest of the compounds showed a reduction in edema formation, but it was smaller than the positive controls. The results in edema reduction are similar to those reported with a series of 2-methylamino-1*H*-benzimidazole derivatives particularly with the *N*-(1*H*-benzimidazol-2-ylmethyl)-3-chloroaniline.[23]

3. Conclusions.

Benzimidazoles are important pharmacophores with a myriad of clinical applications. Although 1,2-diphenylbenzimidazole compounds are not structurally related with conventional anti-inflammatory drugs, including NSAIDs or Coxibs, the *in-silico* studies herein reported demonstrated that some of the synthetized compounds bind to similar sites that the Coxibs. The N1-Ph substitution increased the selectivity towards COX-2 by producing a differential binding mode in each isoform. Moreover, the different *para* substitutions at the 1,2-diphenilbenzimidazole structure allowed to obtain a handful of selective active compounds to different pharmacological targets. The *para*-NO_2 and *para*-Br at N1-Ph and *C*2-Ph substitutions, respectively, favour the inhibition towards COX-2, as seen with the 2-(4-bromophenyl)-1-(4-nitrophenyl)-1*H*-benzo[*d*]imidazole compound. On the other hand, by keeping the halogenated groups in the *C*2-Ph *para* position but functionalizing the N1-Ph *para* position with an acetamide group, a new series of compounds were generated capable to inhibit the secretion of NO as seen with *N*-(4-(2-(4-bromophenyl)-1*H*-benzo[*d*]imidazol-1-yl) phenyl)acetamide and *N*-(4-(2-(4-chlorophenyl)-1*H*-benzo[*d*]imidazol-1-yl)phenyl)acetamide. Importantly, the docking studies towards COX-2 correctly predicted those compounds with the best anti-inflammatory activity in the *in vitro* and *in vivo* assays, although some chemical modification towards the 1,2-DPBIs are necessary to increase the potency of the synthetized compounds. In summary, the functionalization of the 1,2-diphenylbenzimidazole scaffold represents a unique opportunity for the synthesis of diverse compounds which target different anti-inflammatory pathways that might lead to the development of new anti-inflammatory drugs.

4. Experimental.

4.1. Instrumental and chemicals.

The uncorrected melting points were measured in open capillary tubes in an Electrothermal apparatus IA 9100. ^{1}H (300.01 MHz) and

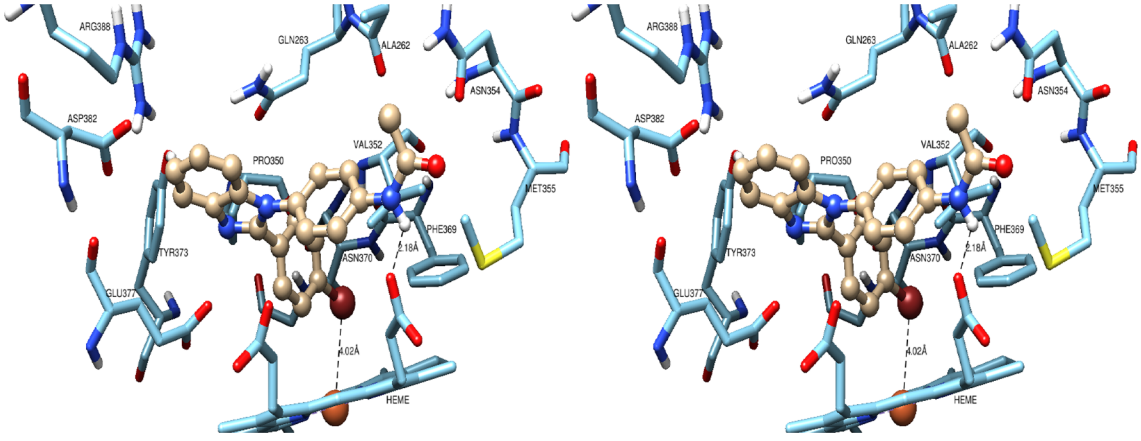

Figure 4. Interaction profiles of compounds **4b** (left) and **4c** (right) in the h-iNOS active site.

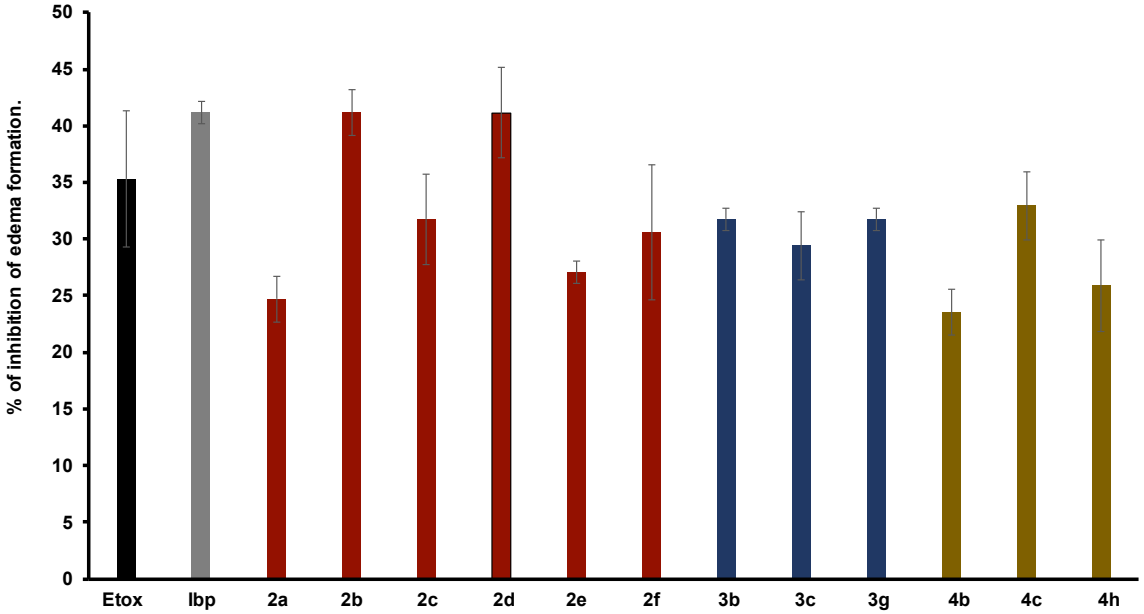

Figure 5. Anti-inflammatory activity of DPBI-substituted compounds *in vivo* orally administered in a rat paw edema model using a dose of 100 mg/kg. Results are present as the mean ± standard deviation of a triplicate of five independent experiments.

^{13}C NMR (75.46 MHz) spectra were recorded on a Varian Mercury-300 spectrometer, except compound **4h** which was recorded on a Bruker (400 MHz ^{1}H, 75 MHz ^{13}C), at 20 °C using $CDCl_3$ as solvent, unless otherwise is specified, and tetramethylsilane (TMS) as internal reference; chemical shift values (δ) are in parts per million (ppm) and coupling constants (^{n}J values) are in Hertz (Hz). IR spectra were obtained neat with a 3100 FT–IR Excalibur Series spectrophotometer. All chromatographic purifications were performed with silica gel (200 –300 mesh), whereas all TLC developments were performed on silica gel coated (Merck 60 F254) aluminium foils. Yields reported are isolated yields of the materials. To indicate the multiplicity of the signals, the abbreviations are used: s, for a simple signal; d, for a double signal; dd, for a double of doubles signal; t, for a triple signal; q, for a quadruple signal; m, for a multiple signals, or different combinations of the above.

X-Ray structure determination. General crystallographic data for compound **2c** has been deposited in the Cambridge Crystallographic Data Centre (CCDC) as supplementary publication number 1963116. Crystal data, collection and refinement parameters are listed in Table S5. Single crystal X-ray diffractions data was collected on an Agilent Super Nova (dual source). The cell refinement and data reduction were carried out with the CrysAlisPro software. The structure was solved by direct methods using the SHELXS-97 program[24] of the WINGX package.[25] The final refinement was performed by full-matrix least-squares methods using the SHELX97 program.[24] The H atoms on C were geometrically positioned and treated as riding atoms with: C − H 0.93 Å, Uiso(H) = 1.2 eq(C) for carbon atoms. Platon[26] and Mercury[27] were used to prepare the material for publication.

Mass analysis was performed by Electro Spray Ionization in a High-Resolution Mass spectrometry Bunker micrOTQF–QII instrument (Brunker Daltonik GmbH, Bremen, Germany).

4.2. Chemical synthesis of DPBI-substituted compounds.

All reagents and solvents were purchased from commercial suppliers and were dried and purified when necessary by standard techniques. Compounds **1a-e** are known but they are not commercially available. Therefore, they were synthesized following the methodology described elsewhere with modifications.[13] The general procedure for the synthesis of **1a-1e** is briefly described: a mixture of o-phenylenediamine (2 mmol), aryl aldehyde (2 mmol) and sodium metabisulfite (2.02 mmol) in 5 mL of DMSO were heated at 140 °C for 2 h. After the completion of the reaction, cold water (50 mL) was added. The resulting precipitate was filtered, washed with plenty of water and air dried. Their spectroscopic properties were in agreement with reported values: compounds **1a**, **1b**, **1c**, **1e**[28–29] and **1d**[30] see SI.

Compounds **2b** and **2e** are known, the first was prepared as reported[13] and the second following the methodology herein described, the data agrees with reported values[31], see SI.

4-(1-(4-nitrophenyl)-1H-benzo[*d*]imidazol-2-yl)benzonitrile (**2a**). In a 100 mL round bottom flask were placed 0.645 g (2.94 mmol) of 4-(1H-benzo[*d*]imidazol-2-yl)benzonitrile (**1a**), 0.406 g (2.94 mmol) of anhydrous K_2CO_3 and 20 mL of DMF. The flask, equipped with a condenser, was heated to 70 °C during 15 min and then 0.35 mL (0.457 g, 3.24 mmol) of 1-fluoro-4-nitrobenzene were added. The reaction mixture was heated to 120 °C, during 48 h under magnetic stirring, left to cool to RT and poured into 50 mL of cold distilled water acidified with 10 drops of concentrated HCl. The resulting solid was filtered, washed with distilled water and dried at RT to obtain 0.650 g of **2a**. The raw product was purified by column chromatography (Hexane/AcOEt 80:20) to obtain 0.40 g (1.47 mmol) of a yellow solid in 50% yield (m.p. 198–200 °C). ^{1}H NMR: δ 8.40 (m AÁ, 2H, H-12,14), 7.91 (dd, 1H, H-4, ^{3}J = 7.0, ^{4}J = 1.0), 7.64 (s, 4H, H-17,18,20,21), 7.50 (m XX́, 2H, H-11,15), 7.42 (dt, 1H, H-5, ^{3}J = 7.5, ^{4}J = 2.0), 7.36 (dt, 1H, H-6, ^{3}J = 7.5, ^{4}J = 2.0), 7.30 (dd, 1H, H-7, ^{3}J = 7.0, ^{4}J = 2.0 Hz). ^{13}C NMR: δ 149.8 (*C*2), 147.4 (C13), 143.1 (C16), 141.9 (C10), 136.4 (C9), 133.6 (C8), 132.4 (C18,20), 130.0 (C17,21), 127.9 (C11,15), 125.7 (C12,14), 124.9 (C6), 124.3 (C5), 120.8 (C4), 118.0 (C22), 113.6 (C19), 110.1 (C7). IR (ν, cm^{-1}): 2225 (C≡N), 1584 (C═C Ar), 1516, 1346 (NO_2), 839, 748 (C−H Ar out of plane). ESI: $[M + H]^{+}$ 341.1029 found, 341.1039 calcd.

2-(4-chlorophenyl)-1-(4-nitrophenyl)-1H-benzo[*d*]imidazole (**2c**). Prepared and purified as described for **2a**, from 2-(4-chlorophenyl)-1H-benzo[*d*]imidazole (**1c**) (0.694 g, 2.42 mmol), 1-fluoro-4-nitrobenzene (0.399 g, 2.83 mmol) and K_2CO_3 (0.351 g, 2.54 mmol) as a yellow solid in 75% yield (m.p. 166– 167 °C). ^{1}H NMR: δ 8.38 (m, 2H, H-12,14), 7.88 (d, 1H, H-4, ^{3}J = 8.0), 7.48 (m, 2H, H-11,15), 7.45 (m, 2H, H-18,20), 7.38 (m, 1H, H-5), 7.33 (m, 2H, H-6,7), 7.32 (m, 2H, H-17,21). ^{13}C NMR: δ 150.8 (*C*2), 146.9 (C13), 142.9 (C16), 142.0 (C10), 136.1 (C9), 135.9 (C8), 130.5 (C18,20), 128.8 (C17,21), 127.7 (C11,15),

127.4 (C19), 125.2 (C12,14), 124.1 (C6), 123.7 (C5), 120.2 (C4), 109.7 (C7). IR (ν, cm^{-1}): 1588 (C=C Ar), 1514, 1348 (NO_2), 834, 771, 746 (C−H Ar out of plane). ESI: $[M + H]^+$ 350.0693 found, 350.0697 calcd.

1,2-bis(4-nitrophenyl)-1H-benzo[*d*]imidazole (**2d**). Prepared and purified as described for **2a**, from 2-(4-nitrophenyl)-1H-benzo[*d*]imidazole (2.00 g, 8.37 mmol), 1-fluoro-4-nitrobenzene (**1d**) (1.42 g, 10.04 mmol) and K_2CO_3 (1.157 g, 8.37 mmol) as a yellow solid in 71% yield (m.p. 234–236 °C). ^{1}H NMR: δ 8.10 (d, 2H, H-12,14, ^3J = 8.9), 7.92 (d, 2H, H-18,20, ^3J = 8.8), 7.57 (m, 1H, H-4), 7.48 (d, 2H, H-11,15, ^3J = 8.9), 7.45 (d, 2H, H-17,21, ^3J = 8.8), 7.08 (m, ^{3}H, H-5,6,7). ^{13}C NMR: δ 149.8 (*C*2), 147.8 (C19), 147.1 (C13), 142.7 (C16), 141.5 (C9), 136.5 (C10), 135.5 (C8), 131.7 (C6), 130.7 (C18, 20), 128.8 (C17,21), 125.5 (C12,14), 124.6 (C5), 123.7 (C11,15), 120.1 (C4), 110.8 (C7). IR (ν, cm^{-1}): 1588 (C=C Ar), 1508, 1343 (NO_2), 854, 740, 702 (C−H Ar out of plane). ESI: $[M + H]^+$ 361.0972 found, 361.0938 calcd.

4-(1-(4-nitrophenyl)-1H-benzo[*d*]imidazol-2-yl)benzoate (**2f**). In 100 mL bottom flask, equipped with condenser, were refluxed 0.500 g (1.47 mmol) of **2a** and 60 mL of concentrated HCl (37%) during 9 h. After cooling to RT the solution was alkalinized to pH = 5 with NaOH solution (60%). The resulting solid was washed with distilled water and dried at RT to obtain 0.30 g (0.84 mmol, 57% yield) of a pale yellow powder, d.p. = 258 °C. ^{1}H NMR: δ 8.40 (d, 2H, H-12,14, J = 8.9 Hz), 7.92 (d, 2H, H-18,20, ^3J = 8.2), 7.84 (m, 1H, H-4), 7.73 (d, 2H, H-17,21, ^3J = 8.9), 7.57 (d, 2H, H-11,15, ^3J = 8.3), 7.36 (m, 3H, H-5,6,7). ^{13}C NMR: δ 167.2 (C=O), 151.4 (*C*2), 147.4 (C13), 143.2 (C16), 142.2 (C10), 136.8 (C9), 133.5 (C8), 132.5 (C19), 129.9 (C18,20), 129.8 (C17,21), 129.1 (C11,15), 125.8 (C12,14), 124.6 (C6), 123.9 (C5), 120.3 (C4), 111.0 (C7). IR (ν, cm^{-1}): 3410, 2780, 2608 (O−H), 1707 (C=O), 1526, 1348 (NO_2), 1275 (C−O), 861, 788, 761 (C−H Ar out of plane). (ESI): $[M + H]^+$ 360.0965 found, 360.0985 calcd.

4-(2-(4-bromophenyl)-1H-benzo[*d*]imidazol-1-yl)aniline (**3b**). In a 100 mL round bottom flask were placed 60 mL of concentrated HCl and warmed to 60 °C in a water bath, 0.500 g (1.27 mmol) of raw **2b** were added, after 15 min, until complete dissolution, followed by 0.319 g (2.69 mmol) of metallic tin in small portions. The mixture was allowed to react during 2 h, cooled to RT and filtered. The filtrate was cooled into an ice-water bath and alkalinized to pH 12 with NaOH solution (60%). The resulting precipitate was washed to obtain 0.250 g (0.686 mmol) of raw **3b**. Further purification was performed by column chromatography (Hexane/AcOEt 4:6) to obtain 0.228 g (0.624 mmol, 49%) of a beige powder m.p. = 224–225 °C. ^{1}H NMR: δ 7.86 (d, 1H, H-4, ^3J = 7.0), 7.51 (d, 2H, H-18,20, ^3J = 8.5), 7.44 (d, 2H, H-17,21, ^3J = 8.5), 7.27 (m, 3H, H-5,6,7), 7.06 (d, 2H, H-11,15, ^3J = 8.4), 6.76 (d, 2H, H-12,14, ^3J = 8.4), 3.93 (s, 2H, NH_2). ^{13}C NMR: δ 151.5 (*C*2), 147.1 (C13), 142.9 (C16), 137.9 (C9), 131.7 (C18,20), 131.0 (C17,21), 129.3 (C8), 128.5 (C11,15), 127.2 (C10), 124.1 (C19), 123.5 (C6), 123.1 (C5), 119.9 (C4), 115.9 (C12,14), 110.9 (C7). IR (ν, cm^{-1}): 3383, 3316, 3188 (N−H), 1640, 1608 (NH_2), 1520 (C=C Ar), 1280, 1260 (C−N), 831, 742 (C−H Ar out of plane). (ESI): $[M(^{81}Br) + H]^+$ 366.0415 found, 366.045 calcd.

4-(2-(4-chlorophenyl)-1H-benzo[*d*]imidazol-1-yl)aniline (**3c**). Synthesized and purified as described for **3b**, starting from 0.500 g (1.43 mmol) of **2c** and 0.319 g (2.69 mmol) of metallic tin to obtain 0.237 g (0.740 mmol, 52%) of a beige powder, m.p. = 215–217 °C. ^{1}H NMR: δ 7.85 (d, 1H, H-4, ^3J = 7.9), 7.57 (d, 2H, H-18,20, ^3J = 8.6), 7.31 (dd, 2H, H-17,21, J = 7.8, J = 1.4), 7.27 (t, 1H, H-5, ^3J = 1.9), 7.24 (m, 1H, H-6), 7.21 (d, 1H, H-7, ^3J = 7.8), 7.05 (d, 2H, H-11,15, ^3J = 8.6 Hz), 6.74 (d, 2H, H-12,14, ^3J = 8.7), 3.93 (s, 2H, NH_2). ^{13}C NMR: δ 151.5 (*C*2), 147.1 (C13), 142.9 (C10), 137.9 (C9), 135.6 (C8), 130.8 (C18,20), 128.8 (C16), 128.7 (C17,21), 128.5 (C11,15), 127.2 (C19), 123.5 (C6), 123.1 (C5), 119.8 (C4), 115.9 (C12,14), 110.9 (C7). IR (ν, cm^{-1}): 3383, 3304, 3188 (N−H), 1640, 1608 (NH_2), 1514 (C=C Ar), 1280, 1260 (C−N), 834, 743 (C−H Ar out of plane). (ESI): $[M + H]^+$ 320.0952 found, 320.0955 calcd.

4,4′-(1H-benzo[*d*]imidazole-1,2-diyl)dianiline (**3g**). Synthesized and purified as described for **3b**, starting from 1.50 g (4.17 mmol) of **2d** and 1.98 g (16.6 mmol) of metallic tin to obtain 0.662 g (2.20 mmol, 53%) of a brown powder, d.p. = 249 °C. ^{1}H NMR (DMSO-d_6): δ 7.60 (d, 1H, H-4, ^3J = 8.0), 7.25 (d, 2H, H-11,15, ^3J = 8.0), 7.17 (t, 1H, H-5, ^3J = 8.0), 7.11 (t, 1H, H-6, ^3J = 7.0), 7.00 (d, 1H, H-7, ^3J = 7.0), 6.97 (d, 2H, H-17,21, ^3J = 8.0), 6.66 (d, 2H, H-18,20, ^3J = 8.0), 6.45 (d, 2H, H-12,14, ^3J = 8.0), 5.47, 5.45 (s, 4H, NH_2). ^{13}C NMR (DMSO-d_6): δ 153.0 (*C*2), 150.0 (C13), 149.0 (C19), 142.6 (C9), 137.9 (C8), 130.1 (C17,21), 128.1 (C11,15), 124.8 (C10), 122.0 (C5,6), 118.3 (C4), 116.9 (C16), 114.5 (C12,14), 113.1 (C18,20), 110.1 (C7). IR (ν, cm^{-1}): 3423, 3385, 3186 (N−H), 1608 (NH_2), 1520 (C=C Ar), 1275 (C−N), 831, 749 (C−H Ar out of plane). (ESI): $[M + H]^+$ 301.1452 found, 301.1454 calcd.

N-(4-(2-(4-bromophenyl)-1H-benzo[*d*]imidazol-1-yl)phenyl)acetamide (**4b**). In a 100 mL round bottom flask, immersed in an ice-water bath, were placed 1.00 g (2.75 mmol) of compound **3b**, 40 mL of THF and 1 mL of TEA. Under vigorous stirring, 1.4 mL of acetyl chloride were added, the reaction mixture was left under stirring for 2 h to reach RT. The solvent was evaporated and the remaining solid was washed with distilled water and dried at RT to obtain 0.900 g (1.99 mmol, 90%) of a beige solid m.p. = 153–156 °C. ^{1}H NMR: δ 10 (s, 1H, NH), 7.86 (d, 1H, H-4, ^3J = 8.0), 7.68 (d, 2H, H-11,15, ^3J = 8.8), 7.60 (b, 1H, H-7), 7.43 (s, 4H, H-17,18,20,21), 7.34 (dt, 1H, H-5, ^3J = 7.5, ^4J = 2.0), 7.28 (dt, 1H, H-6, ^3J = 7.5, ^4J = 2.0), 7.26 (d, 1H, H-12,14, ^3J = 8.0), 7.25 (d, 1H, H-7, ^3J = 8.0), 2.22 (s, 3H, CH_3). ^{13}C NMR: δ 168.5 (C=O), 151.2 (*C*2), 142.7 (C16), 138.4 (C13), 137.3 (C9), 132.2 (C8), 131.6 (C18), 130.8 (C17), 128.7 (C10), 127.9 (C11,15), 124.2 (C19), 123.7 (C6), 123.3 (C5), 120.8 (C12,14), 119.8 (C4), 110.5 (C7), 24.7 (CH3). IR (ν, cm^{-1}): 3465 (N−H), 1667 (C=O), 1594 (C=C Ar), 1264 (C−N), 821, 746 (C−H Ar out of plane). (ESI): $[M + H]^+$ 406.0588 found, 406.0556 calcd.

N-(4-(2-(4-chlorophenyl)-1H-benzo[*d*]imidazol-1-yl)phenyl)acetamide (**4c**). Synthesized and purified as described for **4b**, starting from 1.50 g (4.69 mmol) of **3c** and 1.5 mL of acetyl chloride to obtain 1.38 g (3.81 mmol, 92%) of a beige powder, m.p. = 154–156 °C. ^{1}H NMR (DMSO-d_6): δ 9.94 (s, 1H, NH), 7.42 (d, 3H, H-4,11,15, ^3J = 8.6), 7.18 (d, 2H, H-18,20, ^3J = 8.6), 7.09 (d, 1H, H-17,21, ^3J = 8.6), 6.99 (d, 2H, H-12,14, ^3J = 8.7), 6.94 (t, 1H, H-5, ^3J = 7.4), 6.91 (t, 1H, H-6, ^3J = 7.0), 6.83 (m, 1H, H-7), 1.72 (s, 3H, CH_3). ^{13}C NMR (DMSO-d_6): δ 168.8 (C=O), 150.7 (*C*2), 142.1 (C9), 139.8 (C13), 137.2 (C10), 134.5 (C8), 131.9 (C16), 130.8 (C18,22), 130.5 (C19), 128.6 (C17,21), 128.0 (C11,15), 123.6 (C5), 123.0 (C6), 120.0 (C12,14), 119.3 (C4), 110.5 (C7), 24.2 (CH_3). IR (ν, cm^{-1}): 3316 (N−H), 1667 (C=O), 1594 (C=C Ar), 1264 (C−N), 841, 750 (C−H Ar out of plane). (ESI): $[M + H]^+$ 362.1046 found, 362.1061 calcd.

N,N'-((1H-benzo[*d*]imidazole-1,2-diyl)bis(4,1-phenylene))diacetamide (**4h**). Synthesized and purified as described for **4b**, starting from 1.50 g (5.00 mmol) of **3 g** and 1.5 mL of acetyl chloride to obtain 0.920 g (2.39 mmol, 48%) of a beige powder, d.p. = 284 °C. ^{1}H NMR (DMSO-d_6): δ 10.45 (s, 2H, NH), 7.91 (d, 1H, H-4, ^3J = 8.0), 7.84 (d, 2H, H-11,15, ^3J = 8.0), 7.69 (d, 2H, H-17,21, ^3J = 8.0), 7.54 (d, 2H, H-18,20, ^3J = 8.0), 7.50 (d, 2H, H-12,14, ^3J = 9.0), 7.56 (t, 2H, H-5,6, ^3J = 7.0), 7.37 (d, 1H, H-7, ^3J = 7.0), 2.1, 2.0 (s, 6H, CH_3). ^{13}C NMR (DMSO-d_6): δ 169.5 (C=O), 150.1 (*C*2), 143.3 (C19), 141.5 (C13), 135.5 (C10), 132.9 (C9), 131.4 (C8), 128.6 (C11,15), 128.3 (C12,14), 117.8 (C16), 128.6 (C17,21), 128.0 (C18), 123.6 (C6), 122.9 (C5), 119.3 (C4), 110.7 (C7), 24.1 (C24,27). IR (ν, cm^{-1}): 3251 (N−H), 1707 (C=O), 1594 (C=C Ar), 1250 (C−N), 844, 755 (C−H Ar out of plane). (ESI): $[M + H]^+$ 385.1655 found, 385.1665 calcd.

4.3. Modelling and in silico studies.

The affinities towards COX-1, COX-2 and h-iNOS enzymes of the set of DPBIs were studied by theoretical means using the Autodock 4.2 program suit to perform molecular docking calculations.[32] The

crystallographic structure of each enzyme was obtained from the Protein Data Bank (PDB Ids: 1EQG, COX-1; 4PH9, COX-2; and 3EJ8, h-iNOS).[33,34]

Both COX models were co-crystallized with the inhibitor ibuprofen, considered together with etoricoxib as references in the calculations. A re-docking calculation on the crystallographic complexes of Ibuprofen with COX-1 and COX-2 was performed to validate the models. The RMSD for the calculated complexes relative to PDB models 1EQG and 4PH9 were 0.883 and 0.803 Å, respectively. Figure S1 compares experimental and calculated docked structures of ibuprofen. The observed RMSD below 0.9 Å confirm that the bioactive conformations are sufficiently well reproduced. Thus, docking calculations on these models are reliable.

The structures of COXs and h-iNOs enzymes were cleaned up by removing small molecules, the chain A of the homodimer including its bounded heme prosthetic group were conserved for COXs enzymes. A standard preparation procedure with the AutoDockTools program followed, where polar hydrogen atoms were added, and Gasteiger atom charges and solvation parameters were assigned. A grid made of 80 × 80 × 80 points with 0.375-Å spacing and centered at the COX inhibitor binding site (i.e. at the center of mass of the crystallographic ibuprofen molecules), defined the volume where the conformational search was performed. Blind docking calculations were performed on h-iNOS, using a 126 × 126 × 126 Å point grid with 0.375 Å spacing centered on the protein. The enzyme-ligand complexes were visualized using AutoDockTools,[33] VMD,[39] and Chimera v1.9.[35]

The protonation state of titratable residues was previously evaluated using the propka-3.1 program,[36] particularly for the His90 residue located inside the COX binding site. Two variants of the neutral form of this residue were used for the docking calculations. It was verified that the same binding modes and energies were in general obtained with both forms. The protonation at the imidazolic Nε of His90 was selected to discuss the results.

The structure of the DPBIs was built and optimized at semiempirical level of theory (AM1) using the Gaussian 09 program.[37] The procedure to prepare the ligands for docking calculations were also carried out with AutoDockTools. Gasteiger atom charges and full flexibility of the ligands was considered. The Lamarkian genetic algorithm was chosen to perform 100 runs (conformational searches) for each ligand and COX isoform. An exhaustive setup was selected to perform the calculation, i.e. 150 individuals as initial population, 27,000 generations, and 2,500,000 energy evaluations. The 100 obtained complexes were structurally clustered with a cutoff of 2 Å in the RMSD to select only the lowest-energy conformation in each cluster for further analysis. The free energy of binding (ΔG°_{b}) of each complex considered in the analysis was estimated with the empirical scoring function of Autodock.[38] Further structural analyses of the obtained complexes were performed by calculating the ligand-receptor contact distance (LRCD) parameter to compare the interaction profile of the studied compounds with the profile of known COX-inhibitor complexes available in structural databases.[9] This screening included 24 COX-1 and 50 COX-2 crystallized complexes from the PDB and aimed to determine similarity with interaction patterns of reference inhibitors

4.4. In vitro and in vivo pharmacological evaluation.

4.4.1. COX-1 and COX-2 enzymatic assays.

COX-1 and −2 inhibition assays were performed according with the manufacturer protocols (Cayman Chemicals). This assay measures the formation of the highly fluorescent compound resorfin generated by the reaction of ADPH (10-acetyl-3,7-dihidroxyphenoxazine) and PGG2 (hydroperoxy endoperoxide) which is formed by the oxidation of AA (araquidonic acid) by COX. Thus, 10 μL of bovine COX-1 and human recombinant COX-2 enzymes were incubated in buffer with the DPBI substituted compounds (100 μM) or specific inhibitors (Dup-697 for COX-2 and SC-560 for COX-1) during 15 and 5 min, respectively. Then, 10 μL of the ADHP and AA were added, and fluorescence was measured after 5 min for both COX-1 and −2 in a plate fluorometer using an excitation/emission light of 530–540/585–595 nm wavelengths.

4.4.2. Determination of the cytotoxicity of DPBI substituted compounds in murine macrophages in vitro using the MTT assay.

Murine macrophages were growth in culture medium composed of RPMI-1640 medium supplemented with 10% of inactivated fetal bovine serum, 2 mmol/L HEPES buffer solution, 100 mM L-glutamine, 100 μg/mL streptomycin, and 100 U/mL penicillin at standard culture conditions 37 °C and 5% CO_2. Cells were counted using a hemocytometer, stained with trypan blue (0.2%) and seeded at concentration of 4 x10^4 cells in 200 μL per well in a 96 well plate with ranging concentrations (0, 50, 100, 150, 200, 250, 300 and 500 μM) of all the compounds dissolved in DMSO (0.2% final concentration) during 24 h. Then, the medium was completely removed, and 100 μL of RPMI with the MTT reagent at a concentration of 0.5 mg/mL was added to each well. The cells were incubated at standard condition for 4 h, centrifuged at 1500 rpm and the solution removed. In the final step, 100 μL of isopropyl alcohol was added, mixed 5 min and read at 570 nm in a plate reader.

4.4.3. Nitric oxide inhibition of the DPBI substituted compounds in murine macrophages activated with LPS

Macrophages were seeded at 4 x10^4 in 200 μL per well in a 96 well plate in culture medium at standard conditions with all the compounds at 50 and 100 μM, and in the presence or absence of LPS (100 ng/mL) overnight. Then, 50 μL of each well was incubated with 50 μL of the Griess reactive and read at 570 nm in a plate reader. The final nitric oxide concentration was calculated using a $NaNO_2$ standard curve at known concentrations.

4.4.4. Anti-inflammatory in vivo activity of DPBI substituted compounds in the paw edema model.

All experiments and protocols described in the present study were conducted according to the Mexican Official Standard NOM-062-ZOO-1999, Technical Specifications for Production, and Care and Use of Laboratory Animals. Healthy male Wistar rats (250–300 g) were procured from the Animal Facility Laboratory at Institute of Neurobiology-UNAM (S7). Animals were housed in polysulfonate cages in groups of 5 animals under controlled conditions of temperature 22 ± 2 °C, relative humidity, 55 ± 5%, and photo-schedule (12 h light, and 12 h dark). Animals had free access to food (Teklad Global Rodent Diet 2018S, Harlan®) and purified water *ad libitum*.

Commercial drugs ibuprofen, etoricoxib and DPBI substituted compounds were administered orally at 10 and 50 mg/kg, respectively, to male Wistar rats (N = 5). One hour after the DPBI substituted compounds were administered, the inflammatory response was induced by injecting 0.1 mL of a 1% carrageenan solution in physiological saline solution on the right paw and volume displacement was recorded at 0, 1, 2, 3, 4, 5 and 6 h after carrageenan administration with a plethysmometer (PLM-01 plus, Orchid Scientific). Difference between the left paw volume and the right paw volume gave the actual edema volumes. The percentage of paw edema inhibition was calculated as the difference in the displaced volume obtained in the treated group and the non-treated group divided by the non-treated group and multiplied by 100 at the different times points.

Acknowledgements

Authors acknowledge the financial support from CONACYT (grant 255354) and the Secretaría de Investigación y Posgrado del Instituto Politécnico Nacional (SIP-IPN). CZG-C thanks the CONACYT Research fellowship 6286 in the project 222. MIG-A and JEG-P also thank CONACYT for the scholarships 407918 and 264544. We also thank to Dr. Susana Rojas-Lima and Dr. José Correa-Basurto for the access to the X-ray and HR-Mass spectrometry instruments, respectively.

Appendix A. Supplementary data

Supplementary data to this article can be found online at https://doi.org/10.1016/j.bmc.2020.115427.

References

1. Rajendran P, Chen Y-F, Chen Y-F, et al. The multifaceted link between inflammation and human diseases. *J Cell Physiol.* 2018;233:6458–6471. https://doi.org/10.1002/jcp.26479.
2. Flower RJ. The development of COX2 inhibitors. *Nat Rev Drug Discov.* 2003;2:179–191. https://doi.org/10.1038/nrd1034.
3. Kirkby NS, Chan MV, Zaiss AK, et al. Systematic study of constitutive cyclooxygenase-2 expression: Role of NF-κB and NFAT transcriptional pathways. *Proc Natl Acad Sci.* 2016;113:434–439. https://doi.org/10.1073/pnas.1517642113.
4. Nissen SE, Yeomans ND, Solomon DH, et al. Cardiovascular Safety of Celecoxib, Naproxen, or Ibuprofen for Arthritis. *N Engl J Med.* 2016;375:2519–2529. https://doi.org/10.1056/NEJMoa1611593.
5. Xu L, Stevens J, Hilton MB, et al. St Croix, COX-2 inhibition potentiates anti-angiogenic cancer therapy and prevents metastasis in preclinical models. *Sci Transl Med.* 2014;6:242ra84. https://doi.org/10.1126/scitranslmed.3008455.
6. Rees DD, Palmer RM, Moncada S. Role of endothelium-derived nitric oxide in the regulation of blood pressure. *Proc. Natl. Acad. Sci. USA.* 1989;86:3375–3378. https://doi.org/10.1073/pnas.86.9.3375.
7. Minhas R, Bansal Y, Bansal G. Inducible nitric oxide synthase inhibitors: a comprehensive update. *Med Res Rev.* 2019. https://doi.org/10.1002/med.21636.
8. Bansal Y, Silakari O. The therapeutic journey of benzimidazoles: A review. *Bioorg. Med. Chem.* 2012;20:6208–6236. https://doi.org/10.1016/J.BMC.2012.09.013.
9. Gómez-Castro CZ, López-Martínez M, Hernández-Pineda J, Trujillo-Ferrara JG, Padilla-Martínez II. Profiling the interaction of 1-phenylbenzimidazoles to cyclooxygenases. *J. Mol. Recognit.* 2019;e2801. https://doi.org/10.1002/jmr.2801.
10. Paramashivappa R, Phani Kumar P, Subba Rao PV, Srinivasa Rao A. Design, synthesis and biological evaluation of benzimidazole/benzothiazole and benzoxazole derivatives as cyclooxygenase inhibitors. *Bioorg Med Chem Lett.* 2003;13(4):657–660. https://doi.org/10.1016/S0960-894X(02)01006-5.
11. Gaba M, Singh D, Singh S, Sharma V, Gaba P. Synthesis and pharmacological evaluation of novel 5-substituted-1-(phenylsulfonyl)-2-methylbenzimidazole derivatives as anti-inflammatory and analgesic agents. *Eur J Med Chem.* 2010;45:2245–2249. https://doi.org/10.1016/J.EJMECH.2010.01.067.
12. Arora RK, Kaur N, Bansal Y, Bansal G. Novel coumarin–benzimidazole derivatives as antioxidants and safer anti-inflammatory agents. *Acta Pharm. Sin. B.* 2014;4:368–375. https://doi.org/10.1016/J.APSB.2014.07.001.
13. González-Padilla JE, Rosales-Hernández MC, Padilla-Martínez II, García-Báez EV, Rojas-Lima S, Salazar-Pereda V. π-stacking and C—*X*...*D* (X = H, NO_2; *D* = O, π) interactions in the crystal network of both C—H...N and π-stacked dimers of 1,2-bis(4-bromophenyl)-1*H*-benzimidazole and 2-(4-bromophenyl)-1-(4-nitrophenyl)-1*H*-benzimidazole. *Acta Crystallogr. Sect. C Struct. Chem.* 2014;70:55–59. https://doi.org/10.1107/S2053229613033329.
14. Gandour RD. Handbook of Reagents for Organic Synthesis; Oxidizing and Reducing Agents. *J Nat Prod.* 2000;63:1596. https://doi.org/10.1021/np990739q.
15. Singh UC, Kollman PA. An approach to computing electrostatic charges for molecules. *J. Comput. Chem.* 1984;5:129–145. https://doi.org/10.1002/jcc.540050204.
16. Kurumbail RG, Stevens AM, Gierse JK, et al. Structural basis for selective inhibition of cyclooxygenase-2 by anti-inflammatory agents. *Nature.* 1996;384:644–648. https://doi.org/10.1038/384644a0.
17. Romero-Castro A, León-Rivera I, Ávila-Rojas LC, Navarrete-Vázquez G, Nieto-Rodríguez A. Synthesis and preliminary evaluation of selected 2-aryl-5(6)-nitro- 1H-benzimidazole derivatives as potential anticancer agents. *Arch. Pharm. Res.* 2011;34:181–189. https://doi.org/10.1007/s12272-011-0201-5.
18. Castrejon JL, Lavergne SN, El-Sheikh A, et al. Metabolic and Chemical Origins of Cross-Reactive Immunological Reactions to Arylamine Benzenesulfonamides: T-Cell Responses to Hydroxylamine and Nitroso Derivatives. *Chem. Res. Toxicol.* 2010;23:184–192. https://doi.org/10.1021/tx900329b.
19. Montesano Ruggero, Pegg Anthony E, Margison Geoffrey P. Alkylation of DNA and carcinogenicity of N-nitroso compounds. *Journal of Toxicology and Environmental Health.* 1980;6(5-6):1001–1008. https://doi.org/10.1080/15287398009529922.
20. Savjani JK, Mulamkattil S, Variya B, Patel S. Molecular docking, synthesis and biological screening of mefenamic acid derivatives as anti-inflammatory agents. *Eur. J. Pharmacol.* 2017;801:28–34. https://doi.org/10.1016/j.ejphar.2017.02.051.
21. Fantacuzzi M, Maccallini C, Di Matteo M, et al. Screening of NOS activity and selectivity of newly synthesized acetamidines using RP-HPLC. *J Pharm Biomed Anal.* 2016;120:419–424. https://doi.org/10.1016/j.jpba.2015.11.045.
22. Garcin ED, Arvai AS, Rosenfeld RJ, et al. Anchored plasticity opens doors for selective inhibitor design in nitric oxide synthase. *Nat Chem Biol.* 2008;4:700–707. https://doi.org/10.1038/nchembio.115.
23. Achar KCS, Hosamani KM, Seetharamareddy HR. In-vivo analgesic and anti-inflammatory activities of newly synthesized benzimidazole derivatives. *Eur J Med Chem.* 2010;45:2048–2054. https://doi.org/10.1016/j.ejmech.2010.01.029.
24. Sheldrick GM. A short history of SHELX. *Acta Crystallogr. Sect. A Found. Crystallogr.* 2008;64:112–122. https://doi.org/10.1107/S0108767307043930.
25. Farrugia LJ. WinGX and ORTEP for Windows: An update. *J. Appl. Crystallogr.* 2012;45:849–854. https://doi.org/10.1107/S0021889812029111.
26. Spek AL. Structure validation in chemical crystallography. *Acta Crystallogr. Sect. D Biol. Crystallogr.* 2009;65:148–155. https://doi.org/10.1107/S090744490804362X.
27. Macrae Clare F, Bruno Ian J, Chisholm James A, Edgington Paul R, McCabe Patrick, Pidcock Elna, Rodriguez-Monge, et al. Mercury CSD 2.0 - New features for the visualization and investigation of crystal structures. *J Appl Crystallogr.* 2008;41(2):466–470. https://doi.org/10.1107/S0021889807067908.
28. Alapati MLPR, Abburi SR, Mukkamala SB, Krishnaji Rao M. Simple and Efficient One-Pot Synthesis of 2-Substituted Benzimidazoles from θ-Diaminoarene and Aryl Aldehydes. *Synth. Commun.* 2015;45:2436–2443. https://doi.org/10.1080/00397911.2015.1083581.
29. Peng J, Ye M, Zong C, et al. Copper-catalyzed intramolecular C-N bond formation: A straightforward synthesis of benzimidazole derivatives in water. *J Org Chem.* 2011;76:716–719. https://doi.org/10.1021/jo1021426.
30. Eshghi H, Rahimizadeh M, Shiri A, Sedaghat P. One-pot synthesis of benzimidazoles and benzothiazoles in the presence of Fe(HSO4)3 as a new and efficient oxidant. *Bull Korean Chem Soc.* 2012;33:515–518. https://doi.org/10.5012/bkcs.2012.33.2.515.
31. Kumar RK, Punniyamurthy T. Palladium-catalyzed aerobic oxidative C-H amination: synthesis of 2-unsubstituted and 2-substituted N-aryl benzimidazoles. *RSC Adv.* 2012;2:4616. https://doi.org/10.1039/c2ra20328f.
32. Morris GM, Goodsell DS, Halliday RS, et al. Automated docking using a Lamarckian genetic algorithm and an empirical binding free energy function. *J. Comput. Chem.* 1998;19:1639–1662. https://doi.org/10.1002/(SICI)1096-987X(19981115)19:14<1639::AID-JCC10>3.0.CO;2-B.
33. Selinsky BS, Gupta K, Sharkey CT, Loll PJ. Structural analysis of NSAID binding by prostaglandin H 2 synthase: Time-dependent and time-independent inhibitors elicit identical enzyme conformations. *Biochemistry.* 2001;40:5172–5180. https://doi.org/10.1021/bi010045s.
34. Orlando BJ, Lucido MJ, Malkowski MG. The structure of ibuprofen bound to cyclooxygenase-2. *J. Struct. Biol.* 2015;189:62–66. https://doi.org/10.1016/j.jsb.2014.11.005.
35. Pettersen EF, Goddard TD, Huang CC, et al. UCSF Chimera - A visualization system for exploratory research and analysis. *J. Comput. Chem.* 2004;25:1605–1612. https://doi.org/10.1002/jcc.20084.
36. Olsson MHM, SØndergaard CR, Rostkowski M, Jensen JH. PROPKA3: Consistent treatment of internal and surface residues in empirical p K a predictions. *J. Chem. Theory Comput. 7.* 2011:525–537. https://doi.org/10.1021/ct100578z.
37. M J Frisch, G W Trucks, H B Schlegel, G E Scuseria, M A Robb, J R Cheeseman, G Scalmani, V Barone, G A Petersson, H Nakatsuji, X Li, M Caricato, A Marenich, J Bloino, B G Janesko et al. Gaussian 09 Revision A.02, 2013, Gaussian, Inc., Wallingford CT.
38. Huey R, Morris GM, Olson AJ, Goodsell DS. Software news and update a semi-empirical free energy force field with charge-based desolvation. *J. Comput. Chem.* 2007;28:1145–1152. https://doi.org/10.1002/jcc.20634.
39. Humphrey W, Dalke A, Schulten K. VMD: Visual molecular dynamics. *Journal of Molecular Graphics.* 1996;14(1):33–38. https://doi.org/10.1016/0263-7855(96)00018-5.